Earthquake triggering in southern Iceland following the June 2000, Ms 6.6 doublet

Guillaume Daniel, David Marsan, Michel Bouchon

Earthquake triggering in southern Iceland following the June 2000 M_s 6.6 doublet

G. Daniel,[1] D. Marsan,[2] and M. Bouchon[1]

Received 11 April 2007; revised 10 January 2008; accepted 29 January 2008; published 24 May 2008.

[1] In June 2000, two remarkably similar M_s 6.6 earthquakes stroke southern Iceland in the space of 3 d. Here this doublet is analyzed to test whether aftershock triggering is linear, that is, if the triggering patterns of these two similar main shocks are also similar. Methodologically, the key issue is to separate the two contributions to the overall seismicity patterns. For this purpose, we model the first 3 d (17–21 June) of this aftershock sequence with an Omori-Utsu law. We then extrapolate it beyond 21 June in order to estimate the variations linked with the second shock. We correct for the large transient changes in catalogue completeness. Our results indicate that instantaneous short-lived (hours to days) dynamic triggering took place at the Hengill Triple Junction, on the Reykjanes Peninsula, and around the Árnes fault plane that ruptured on 17 June. We observe delayed, long-lasting (longer than weeks) episodes of quiescence at Hengill and on the Árnes fault plane. At Hengill this quiescence remains significant up to at least the end of 2000. These quiescences are more consistent with Coulomb stress calculations than the preceding episodes of triggering. Comparison between the number of triggered events by the two main shocks reveals that the second one triggered only 2.1% at Hengill and 0.3% at Reykjanes of the number (3.6% and 0.1%, respectively, of the seismic moment) that could be expected with a simple stress threshold model of dynamic triggering. This clear nonlinearity in patterns of dynamic triggering is consistent with a model in which the population of nucleating earthquakes is depleted by the first trigger.

Citation: Daniel, G., D. Marsan, and M. Bouchon (2008), Earthquake triggering in southern Iceland following the June 2000 M_s 6.6 doublet, *J. Geophys. Res.*, *113*, B05310, doi:10.1029/2007JB005107.

1. Introduction

[2] Stress changes induced by an earthquake are suspected to influence the distribution of off-fault seismicity, and to condition the future occurrence of large earthquakes [*Das and Scholz*, 1981; *King and Cocco*, 2000, and references therein]. These changes are expected to modify the preexisting activity in the surrounding crust. Consequently, the study of seismicity rate changes after a large earthquake offers an opportunity to understand how the crust reacts to a stress perturbation. It has been suggested by a number of recent studies [*Parsons*, 2002; *Marsan*, 2003; *Felzer and Brodsky*, 2005; *Mallman and Zoback*, 2007] that seismicity quiescences, i.e., negative rate changes, are almost nonexistent or rare at the scale of weeks/months. This could be caused by bias in the statistical analysis, as quiescences are not detectable if the prior level of seismicity is too low [*Marsan and Nalbant*, 2005]. A way to reduce this bias is to focus on sequences with several large shocks, so that the seismicity at the time of the later earthquakes is already high. Also, such sequences are particularly interesting as they allow to test whether triggering is intrinsically linear with respect to the time of occurrence of the trigger earthquakes, i.e., if the seismicity patterns caused by a succession of main shocks can be reduced to a simple sum of the individual triggering of each main shock taken separately. Here, we focus on the earthquake doublet that occurred in the Southern Iceland Seismic Zone (SISZ) in June 2000.

[3] The sequence started on 17 June 2000 at 1540:51 UT with a M_s 6.6 right-lateral strike-slip earthquake, which hypocenter was located at 63.97°N, 20.37°W, and 6.3 km depth (Icelandic Meteorological Office (IMO) database, available at http://hraun.vedur.is/cgi-bin/sellib). Aftershock locations indicate that this main shock ruptured the 11 km long Árnes fault characterized by strike N7°E and dip 86°E [*Stefánsson et al.*, 2003]. The second large earthquake had a very similar magnitude (M_s 6.6) and occurred on 21 June at 0051:46.95 UT, i.e., 3.5 d later, on a parallel fault (the Hestfjall fault) located 17 km west of the Árnes fault (see Figure 1).

[4] Several studies have already put forward the interactions existing between earthquakes of this sequence. Calculation of the Coulomb stress changes following the 17 June event reveals an increase of about 1 bar at the 21 June epicenter, thus promoting failure of this second event

[1]Laboratoire de Géophysique Interne et Tectonophysique, CNRS, Université Joseph Fourier, Grenoble, France.
[2]Laboratoire de Géophysique Interne et Tectonophysique, CNRS, Université de Savoie, Le Bourget du Lac, France.

0148-0227/08/2007JB005107$09.00

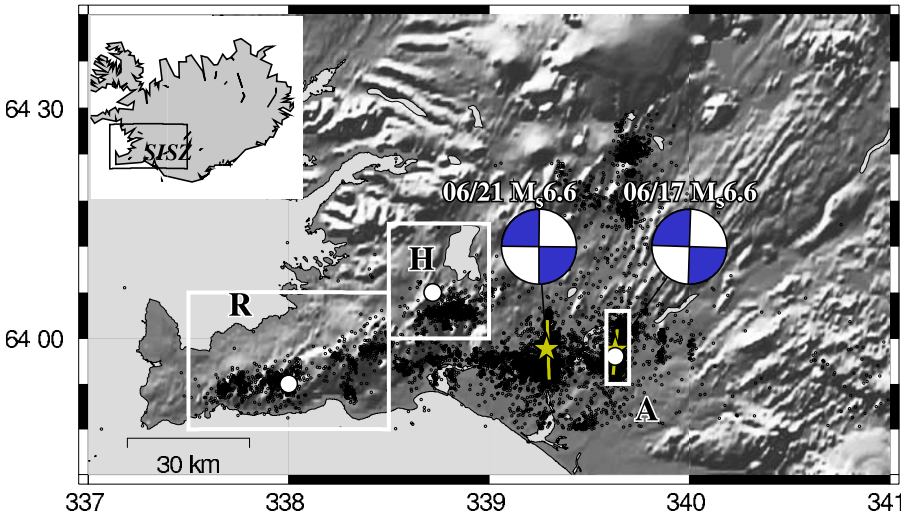

Figure 1. Map of southern Iceland with seismicity from June to December 2000. Areas of investigation are indicated by white rectangles: R, Reykjanes Peninsula; H, Hengill Triple Junction; and A, Árnes fault plane. Lines and stars indicate the 17 and 21 June fault planes and epicenters. White circles point to places where the dynamic stress is calculated. Inset shows location of the Southern Iceland Seismic Zone (SISZ).

[*Árnadóttir et al.*, 2004]. The location of aftershocks also correlates well with zones of increased Coulomb stress, in the vicinity of these two faults. Besides, the 17 June earthquake was followed by quasi-instantaneous (few seconds) $M_L \sim 3.5$ aftershocks occurring at several tens of kilometers from the epicenter. These remote aftershocks could be caused by dynamic triggering related to the passage of the main shock seismic waves [*Clifton et al.*, 2003; *Pagli et al.*, 2003; *Antonioli et al.*, 2006]. *Árnadóttir et al.* [2004] notes that the 21 June earthquake, although being closer, triggered a weaker activity than the 17 June main shock in the Reykjanes Peninsula.

[5] Such a doublet of similar earthquakes (same focal mechanism, same size) occurring in a short time interval and close from each other is remarkable. However, this close succession of large main shocks also brings a particular challenge for the estimation of seismicity rate changes, as the detection threshold of the seismological network is subject to large fluctuations during the period of interest. We overcome this difficulty by modeling the incompletely detected aftershock rate.

[6] In what follows, we use the large number of aftershocks recorded by the South Iceland Lowland (SIL) network [*Jakobsdóttir*, 2006] to document fine changes in microseismic activity linked with these two main shocks. In particular, we study how the stress perturbation induced by the 21 June event affected the seismicity triggered 3 d before by the first main shock. Seismicity rate changes are computed using the approach proposed by *Marsan* [2003], further modified in order to account for rapid changes in completeness magnitude. Discussion of the results obtained for three selected regions in southern Iceland is given in section 3.

2. Investigating Seismicity Rates Variations of an Incomplete Catalogue

[7] We study the catalog from the IMO, which contains about 50,000 seismic events from 1 January 1999 to 31 December 2000. During quiet periods (i.e., before June 2000) this network detects all events with magnitude above $M_c \sim 0.5$ (see Figure 2). *Wyss and Stefánsson* [2006] point out that this completeness level varies spatially, reaching $M_c = 1$ in some parts of the Reykjanes Peninsula. Our estimates, presented on top of Figure 2, are in agreement with this observation. The bottom graph of Figure 2 shows spatially averaged frequency-magnitude distributions of earthquakes for the whole of southern Iceland. After 17 June 2000 the completeness increases substantially in the SISZ because of important aftershock activity and overload of processing facilities (Vogfjörð, K., personal communication, 2006). Following such an increase, one expects the detection threshold to return back to its stationary level within a few days to weeks after the main shock. The short time lapse (3.5 d) between the two main shocks thus implies significant variations in the detection threshold, that need to be properly accounted for in this analysis. Our approach allows the study of seismicity rates during periods of nonstationary M_c level (e.g., between 17 and 21 June), as we now detail.

2.1. General Outline of the Method

[8] We calculate the probability that there exists an increase (or a decrease) of the seismicity rate after a large main shock according to the procedure already described by *Marsan* [2003], *Marsan and Nalbant* [2005], and *Daniel et al.* [2006]. This method is here modified to include all detected seismicity, following *Ogata and Katsura* [2006]. Instead of throwing out many earthquakes (events with magnitude $M < M_c$), we optimize the available information: we use all earthquakes detected by the network, including those events with magnitude lower than the completeness of the catalog M_c. This requires calculating the probability of detection of an earthquake by the seismic network (see section 2.2).

[9] Usually, precursory seismic activity is very weak before large earthquakes, and estimation of rate variations induced by a main shock can be strongly biased toward the

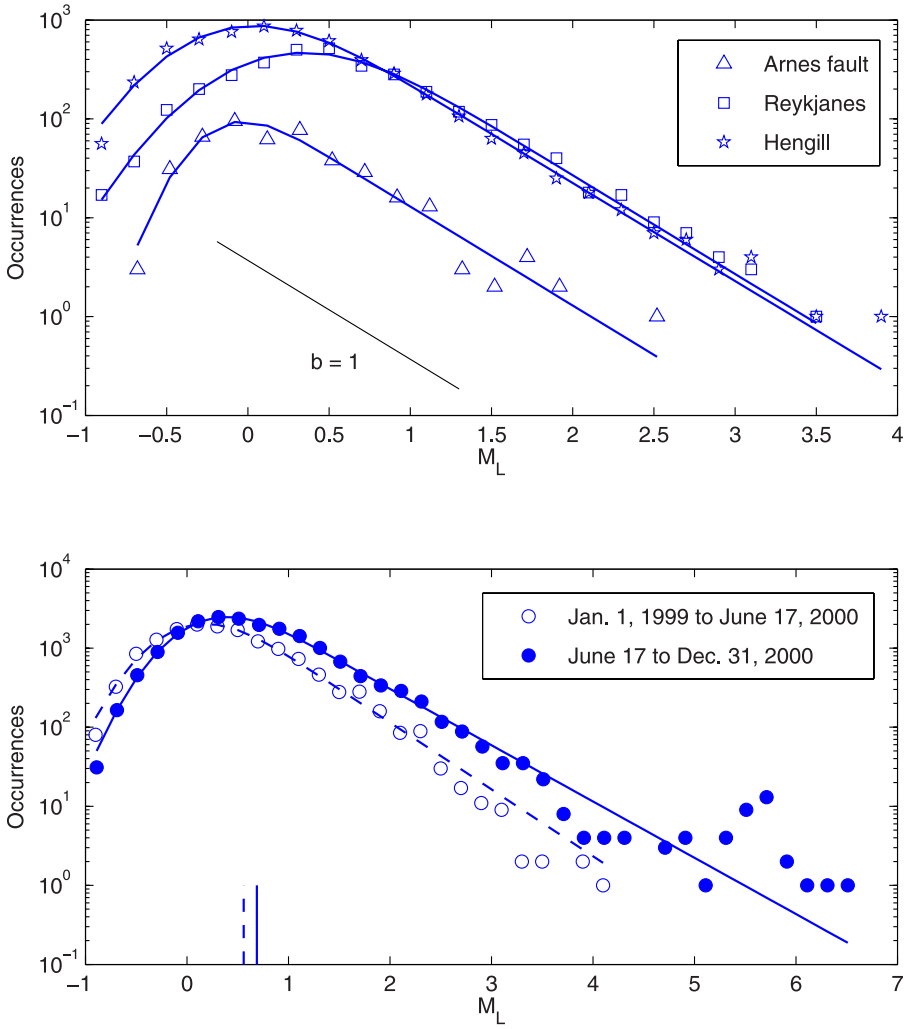

Figure 2. Frequency-magnitude distributions for SIL earthquakes in southern Iceland since 1 January 1999. Lines here show the best fits of the model described by equation (2). (top) Seismicity occurring before 17 June 2000 for the three areas investigated in section 3. The *b* values are reported in Table 1. For this period, completeness level is higher in the Reykjanes Peninsula than at Hengill and Árnes. (bottom) Comparison of the seismicity occurring before and after the June 2000 earthquake doublet, for the whole of southern Iceland. At this regional scale, the completeness level (vertical marks above the axis) increases by 0.13 and *b* value decreases by 0.14 after the doublet.

detection of triggering [*Marsan and Nalbant*, 2005]. Investigating for quiescence consequently requires a high level of seismicity before the main shock. In the case of earthquake doublets, this is achieved when analyzing seismicity rate variations occurring after the second large event. The aftershock sequence initiated by the first main shock is modeled by an Omori-Utsu law, and changes brought by the second- main shock are then estimated by comparing the actual rates to this reference Omori-Utsu rate.

[10] Seismicity is modeled as a Poisson process. The probability of observing n events during an interval of duration δt is

$$P(n|\Lambda) = e^{-\Lambda}(\Lambda^n/n!)$$

with $\Lambda = \int_t^{t+\delta t} \lambda(s)\, ds$, and $\lambda(t)$ is the seismicity rate at time t.

[11] *Marsan* [2003] estimates changes in seismicity rate as follows:

[12] 1. Adjustment of the reference seismicity rate $\lambda_0(t)$ for the period spanning from the first main shock up to the second one. In this analysis, we use the modified Omori-Utsu formula [*Omori*, 1894; *Utsu*, 1961] for $\lambda_0(t)$:

$$\lambda_0(t) = \frac{K}{(t+c)^p} \tag{1}$$

[13] 2. Extrapolation of $\lambda_0(t)$ after the second main shock. This extrapolation represents the seismic activity that would be expected if the second main shock had not occurred.

[14] 3. Comparison of the extrapolated rate $\lambda_0(t)$ with the actual observed rate $\lambda_1(t)$ after the second main shock. We characterize the perturbation (triggering/quiescence) by comparing this expected seismicity rate $\lambda_0(t)$ with the pdf

Table 1. Summary of Parameters Estimate for the Synthetics and for the Three Areas of Investigation[a]

	Synthetics	Estimate	Hengill	Reykjanes Peninsula	Árnes Fault
Longitude min, max	–	–	[−21.5; −21]	[−22.5; −21.5]	[−20.415; −20.3]
Latitude min, max	–	–	[64; 64.25]	[63.8; 64.1]	[63.9; 64.06]
$M_{\min}$	–	0	1	1	0
K	2000	1981 ± 73	195 ± 15	188 ± 15	1831 ± 98
p	1	0.97 ± 0.01	1.45 ± 0.07	1.45 ± 0.06	1.08 ± 0.04
b	–	–	1.00 ± 0.07	1.00 ± 0.08	0.99 ± 0.17
T_{start}, d	–	–	0.1	0.04	0.34
K_2	–	–	1.8 ± 11.1	0.4 ± 2.7	0 ± 1210
p_2	–	–	1.43 ± 1.41	1.47 ± 1.41	1.06 ± 1.41

[a]Note that parameter c from the modified Omori formula is set to 0.003 d.

of the actual seismicity rate $f_1(\lambda_1)$. This pdf is expressed as the probability that the n observed events in the target time interval result from a Poisson process with mean $\lambda_1 \delta t$:

$$f_1(\lambda_1) = \delta t e^{-(\lambda_1 \delta t)} \frac{(\lambda_1 \delta t)^n}{n!}$$

We define the probability $\mathcal{P}$ of triggering as the probability that $\lambda_1 > \lambda_0$:

$$\mathcal{P} = \int_0^\infty d\lambda_0 \int_{\lambda_0}^\infty d\lambda_1 f_0(\lambda_0) f_1(\lambda_1)$$

from which we can derive the γ statistics [*Marsan*, 2003] as

$$\gamma = -\text{sgn}(\mathcal{P} - 0.5) \log_{10} [\min(\mathcal{P}, 1 - \mathcal{P})]$$

For example, a probability $\mathcal{P}$ = 99.9% of triggering corresponds to γ = +3 while $\mathcal{P}$ = 0.01% corresponds to γ = −4, which is a 99.99% probability of quiescence. Note that γ and $\mathcal{P}$ are obtained from the comparison of observed and extrapolated rates on a given time interval $[t, t + \delta t]$, and thus uniformly reflect rate changes during the whole time interval.

2.2. Accounting for a Nonstationary Detection Threshold

[15] We model aftershock rate following a main shock with a modified Omori formula (see equation (1)). This empirical law is one of the most robust in seismology, but it should be emphasized here that it only holds for complete data sets. We fitted the best K and p parameters for each area. In order to extend this law to incomplete data sets, we first need to estimate how incomplete is the frequency-magnitude distribution, i.e., what is the probability for an earthquake of magnitude $M < M_c$ to be detected by the network. To do so, we model the frequency distribution $\varphi(M)$ with a Gutenberg-Richter law [*Gutenberg and Richter*, 1954] multiplied by a detection function $q(M)$ [*Ringdal*, 1975; *Ogata and Katsura*, 1993]:

$$\varphi(M) = a\beta e^{-\beta M} q(M) \quad (2)$$

with $\beta = b \log(10)$. The detection function $q(M)$ corresponds to the probability that the network detects a seismic event with magnitude equal to M.

[16] *Ringdal* [1975] proposed modeling this function based on the argument that $q(M)$ is also the probability that the incoming waves radiated by the magnitude M earthquake are significantly above a typical station noise. For a lognormal noise, this leads to $q(M)$ being modeled by the integral of a gaussian distribution. We follow this approach and use

$$q(M > M_{\min}) = \frac{1}{\sigma\sqrt{2\pi}} \int_{M_{\min}}^{M} e^{-\frac{(M-\mu)^2}{2\sigma^2}} dM = 0.5 + 0.5 \text{ erf}\left(\frac{M-\mu}{\sigma\sqrt{2}}\right)$$

$$q(M \le M_{\min}) = 0$$

where μ stands for the magnitude at which a rate of 50 per cent of events are detected. Magnitude of completeness M_c is defined as $\mu + \sigma$, i.e., the magnitude at which 84 per cent of events are detected $M_{\min}$ is the magnitude at which 0 per cent of events are detected.

[17] This frequency-magnitude model for earthquakes fits equally well individual regions, as well as the whole of the Icelandic data set (see Figure 2). We obtained best parameters by maximum likelihood estimation (MLE). These estimates show a global decrease of the b value (from 0.85 to 0.71), and a global increase of the detection threshold $M_c = \mu + \sigma$ (from 0.56 to 0.69) after the June 2000 doublet. Though is has been showed that the b value can change with time [*Wiemer et al.*, 1998; *Wiemer and Katsumata*, 1999], we here interpret this decrease of b as deriving from the high completeness level at short times after the main shocks, as pointed out by *Marsan and Lengliné* [2008], and also as changes in the spatial distribution of earthquakes. Consequently, we run the analysis for southern Iceland with a constant b value for each area (see Table 1) in order to overcome this feature. In doing so, we found the estimate of the completeness to be more stable with time. The b values were first calculated from the magnitude distribution of events occurring before the doublet (see Figure 2, top). These b values are very close or equal to 1 (see Table 1).

[18] In what follows, we use all events above a minimum magnitude $M_{\min}$ equal to 1 in Hengill and in the Reykjanes Peninsula, and to 0 on the Árnes fault. This selection keeps about 80% of all the earthquakes detected by the SIL network, compared to the 39% of events with $M \ge M_c$.

[19] We model the decay rate of aftershocks with $M \ge M_{\min}$. We correct the Omori-Utsu law for incomplete

detection, by multiplying it by a time-dependent probability $\pi(t)$ which is the probability of detecting an earthquake with $M \geq M_{\min}$:

$$(\lambda t) = \frac{K\pi}{(t+c)^p} \tag{3}$$

with,

$$\pi = \int_{M_{\min}}^{\infty} \beta e^{-\beta(M-M_{\min})} q(M)\, dM \tag{4}$$

π can be expressed as

$$\pi = q(M_{\min}) + \exp\left[\left(\sigma^2\beta^2/2\right) - \beta(\mu - M_{\min})\right]\left[1 - q\left(M_{\min} + \sigma^2\beta\right)\right] \tag{5}$$

Because the detection capability of the network changes quickly with time during the June 2000 sequence, the parameters μ and σ of $q(M)$ are time-dependent, ensuring that the probability π also varies with time.

2.3. Practical Implementation of the Method

[20] The variables $\pi(t)$ and $q(M,t)$ are averaged along discretized time windows of N_p = 150 detected events, moving 10 events forward for each new window. For each time window i, we search for the best μ and σ that fit the corresponding frequency-magnitude distribution of these N_p events. The probability density function φ for the magnitude of detected events is given in equation (2). Parameter a of equation (2) is optimized by setting

$$\int_{M_{\min}}^{+\infty} \varphi(M)\, dM = N_p \tag{6}$$

Thus, for the ith time window (with duration $\delta\, t_i = t_i - t_{i-1}$), the best $\{\mu,\sigma\}$ parameters minimize the following cost function $\mathcal{C}$:

$$\begin{aligned} \mathcal{C} &= N_p - \sum_j v_j \ln \Phi_j \\ \Phi_j &= \int_{M_{\min}+(j-1)\delta M}^{M_{\min}+j\delta M} \varphi(M)\, dM \end{aligned} \tag{7}$$

where v_j is the number of events in which magnitude is in the $[M_{\min} + (j-1)\delta\, M;\ M_{\min} + j\delta\, M]$ interval; $\pi(t)$ is then calculated following equation (5).

[21] According to the model, the mean number of earthquakes detected during the ith time window is

$$\Lambda_i = \int_{t_{i-1}}^{t_i} \frac{K\pi}{(t+c)^p} dt \tag{8}$$

[22] We obtain parameters $\{K,p\}$ of the modified Omori formula by MLE. We set c = 0.003 d($\sim$4 min and 20 s) in order to increase the efficiency of the estimation procedure. This value is of the order of the main shock signal duration (including the coda), during which the detection of smaller events is very difficult. The c parameter thus represents the transition time from a continuum (the main shock) to the discrete occurrence of aftershocks [*Kagan and Knopoff*, 1981]. A nonzero c value is also useful for avoiding rate singularity at $t = 0$. We found that c values greater than 0.01 d lead the MLE to return higher p values, and bias the analysis toward triggering. Estimation of parameters K and p is stable for any c value smaller than this threshold.

[23] The best$\{K,p\}$ parameters maximize the following likelihood function $\mathcal{L}$:

$$\begin{aligned} \mathcal{L} &= \prod_i e^{-\Lambda_i} \frac{\Lambda_i^{n_i}}{n_i!} \\ &= \prod_i \int e^{-\tilde{\Lambda}_i} \frac{\tilde{\Lambda}_i^{n_i}}{n_i!} f_\Lambda\left(\tilde{\Lambda}_i\right) d\tilde{\Lambda}_i \\ &= \prod_i \frac{E\{e^{-\tilde{\Lambda}_i}\tilde{\Lambda}_i^{n_i}\}}{n_i!} \end{aligned} \tag{9}$$

In this expression, the indices i are related to adjacent time windows. n_i gives the number of observed (detected) events, and $\tilde{\Lambda}_i$ is the Poisson mean number of events occurring in the ith time window. The pdf of this number is denoted as $f_\Lambda(\tilde{\Lambda}_i)$. Here, it should be emphasized that we do not recreate any earthquake missed by the network. On the contrary, we rather adapt the rate of the modified Omori formula according to the probability $\pi(t)$ that, at time t, the network is able to detect an earthquake occurring with magnitude $M \geq M_{\min}$. Note also that $\tilde{\Lambda}_i$ is estimated with its distribution, in order to propagate uncertainties on the estimate of $\pi(t)$.

2.4. A Test of the Method

[24] In order to test the method, we built a synthetic data set $\mathcal{D} = \{t_i;\ M_i\}_{i\in[1;\mathcal{N}]}$, containing the occurrences times t_i and the magnitudes M_i of $\mathcal{N}$ events. These earthquakes correspond to aftershocks of two main shocks occurring at times t_a = 0 and t_b = 4, in arbitrary units. Following these two main shocks, we generate two similar Omori-like aftershock sequences. Table 1 summarizes the parameters chosen for this synthetic catalogue. To simulate the effect of a time-varying detection by the network, we decimate the aftershock rates under the hypothesis that the completeness threshold M_c decays exponentially after the main shock (see Figure 3, top). The decimation is done by thinning, according to the probability $q(M,t)$ that an aftershock of magnitude M is detected by the network. This mimics how the catalog completeness increases in the few hours/days following a main shock, and then returns to its "background" level. This choice of an exponentially decaying $M_c(t)$ is dictated by similar observations on real sequences [*Ogata and Katsura*, 2006; *Helmstetter et al.*, 2006].

[25] Once decimated, the remaining aftershocks reproduce the seismicity that would be detected by the network under variable detection threshold.

[26] Using this decimated data set as the input for the method described above, we retrieve the seismicity rate change that occurs after t_b. We first estimate variations of the completeness threshold under a constant b value hypothesis. On Figure 3 (top) we see the good agreement

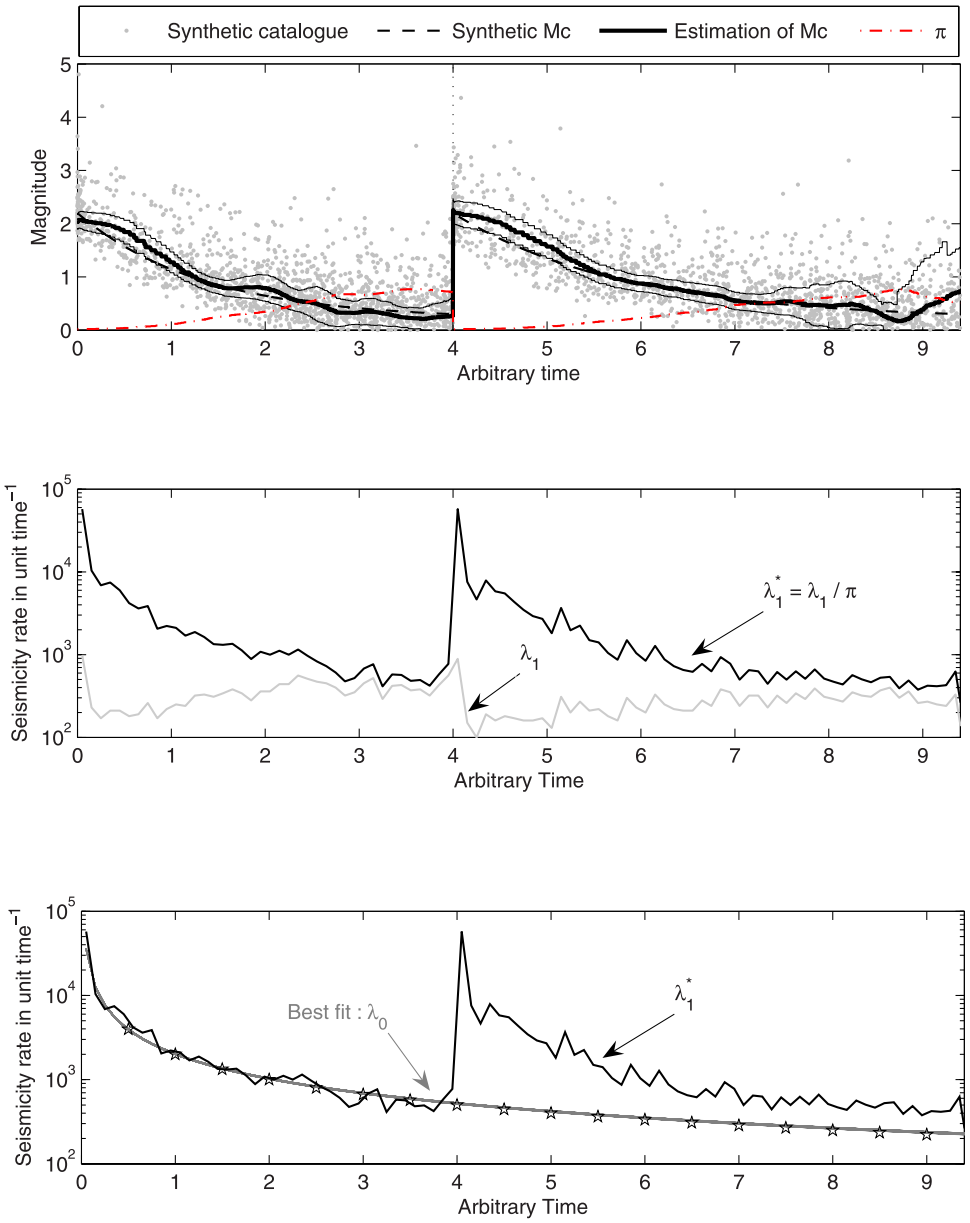

Figure 3. Method. (top) Synthetic catalog of aftershocks obeying the Omori-Utsu formula (see Table 1 for parameters), where the completeness threshold decays exponentially (black dashed line). We estimate $M_c(t)$ (black line, along with errors), using a sliding window of 200 events, moving 10 by 10. From this estimate, we then compute the probability π(t) (dash-dotted line), see equation (5). (middle) Rate $\lambda_1{}^\star$ of earthquakes with $M0$ that would be recorded by the network if completeness were stationary at $M = 0$ (black line). Grey line indicates rate of observed/detected events $\lambda_1(t)$. (bottom) Reconstructed fit of $\lambda_1(t)^\star$ before the second main shock (grey line, with error envelop). Agreement with the synthetic rate before decimation, modified Omori formula (stars), is very good (see Table 1). The seismicity rate change after $t = 4$ is obtained by comparing the extrapolation of this fit (grey line) to the actual rate (black line).

between our estimate and the "true" exponential decay of $M_c(t)$ used for synthetics.

[27] We then estimate the aftershock rate for all events $\lambda_1^\star$, including those undetected, down to $M_{\min}$.

$$\lambda_1^\star(t) = \frac{\lambda_1(t)}{\pi(t)} \tag{10}$$

where $\lambda_1(t)$ is the rate of events down to $M_{\min}$ that were actually detected by the network. Rates are represented on Figure 3 (middle).

[28] We search for the best Omori-Utsu formula $\lambda_0(t) = K/(t + c)^p$, that fits $\lambda_1^\star$. As mentioned in section 2.3, we estimate the $\{K,p\}$ parameters, such that

$$\lambda_1(t) = \frac{K}{(t+c)^p}\pi(t) \tag{11}$$

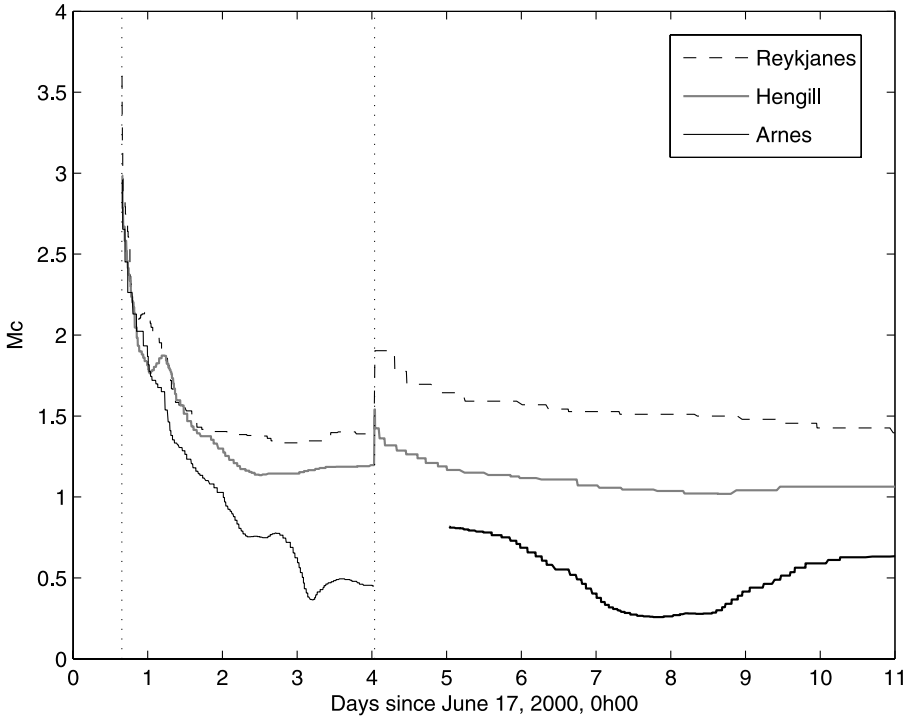

Figure 4. Magnitude of completeness during 10 d after the 17 June earthquake for Árnes (black line), Reykjanes (dashed line), and Hengill (grey line).

Table 1 gives the best values for K and p, which are very close to the true parameters. Figure 3 (bottom) compares $\lambda_1^\star$ and $\lambda_0(t)$ which match closely, as expected. Such good agreement shows that we retrieve the suitable completeness decay, given the function $q(M, t)$. In addition, we obtain the error estimate on the corrected seismicity rate. The adequacy of $q(M, t)$ in describing the data is shown on Figure 2.

[29] Extrapolation of $\lambda_0(t)$ to times longer than t_b is also shown on Figure 3. We compare this model with the rate $\lambda_1^\star$ of earthquakes that would be detected by the network under stationary completeness conditions with $M_c = M_{\min}$:

$$\lambda_1^\star(t > t_b) = \frac{\lambda_1(t > t_b)}{\pi(t > t_b)} \tag{12}$$

The discrepancy between these two rates as seen on Figure 3 (bottom) argues in favor of a triggering episode after t_b. We find a probability $\mathcal{P} > 1 - 10^{-11}$ for triggering ($\gamma > 11$). This proves the ability of the method to properly correct for nonstationary completeness, especially as the rate of detected earthquakes $\lambda_1(t)$ spuriously dips after the second main shock due to an increase of the detection threshold.

3. Rate Changes in Southern Iceland Following the 21 June Earthquake

[30] We investigate changes in seismicity rate after the 21 June earthquake. We particularly focus on three areas distributed in southern Iceland: the Hengill Triple Junction (a volcanic system), the Reykjanes Peninsula, and the 17 June Árnes fault plane (see Figure 1). We selected these areas because of (1) their aftershock activity starting swiftly after the 17 June earthquake, (2) their high aftershock rates and wide coverage allowing for a reliable estimate of the seismicity rate between 17 and 21 June, and (3) the relative coherence of their geological settings. We also studied an area including the Geyser region, but in this case, the paucity of aftershocks between 17 and 21 June did not allow for a reliable estimate of the seismicity rate model.

[31] These three areas exhibit different recoveries of their completeness level M_c after the two June 2000 main shocks (see Figure 4). The Árnes area shows the lowest detection threshold, with $M_c < 1$ starting from 19 June but is characterized by important fluctuations after 21 June. The Hengill and Reykjanes areas both have a higher completeness level ($M_c > 1$) decreasing smoothly with time. We compute the seismicity rates for $M_{\min} = 0$ at Árnes, and for $M_{\min} = 1$ at Hengill and Reykjanes.

[32] Early aftershock rates following the 17 June event exhibit an anomalous feature lasting for a few hours and characterized by a slower decay. This could be linked to an underestimation of $M_c(t)$ for that short period of time, which subsequently caused an overestimation of $\pi(t)$, and an underestimation of $\lambda_1^\star(t)$. For this reason, we only used the aftershock activity starting a few hours (at T_{start}, as indicated in Table 1) after the 17 June event in order to estimate the modified Omori formula parameters K and p. T_{start} is equal to the median time of the first sliding window, after which our estimates of $M_c(t)$ were seen to be reliable on the synthetic test.

[33] We obtain p values ranging from normal ($p = 1.08$ on Árnes fault) to high values ($p \sim 1.5$ for Hengill and Reykjanes). We stress here that peculiar crustal settings, like hydrothermal activity at Reykjanes [*Clifton et al.*, 2003]

Table 2. The γ Statistics Values for Different Target Intervals Following the 21 June Main Shock[a]

Target Period	Hengill	Reykjanes Peninsula	Árnes Fault
[21 June to 21 June + 2 h, 30 min]	14.7	1.6	–
[21 June to 22 June]	14.5	1.5	–
[22 June to 23 June]	0.7	−0.7	2.5
[1 July to 1 Oct]	−4.7	−1.3	−10.1

[a]The first 2 hours and 30 min; the first day; the second day; and between the tenth and the hundredth day after the 21 June earthquake. We cannot estimate any value on 21 June at Árnes because of an artificial gap in the data (see section 3.1).

and volcanic activity at Hengill [*Einarsson*, 1991] might be responsible for the observed fast decay of aftershock activity. Such fast decays have been reported on mid-ocean ridges [*Bohnenstiehl et al.*, 2002] or in the vicinity of calderas [*Klein et al.*, 2006], and have been attributed to high-temperature conditions and fast stress relaxation. This interpretation is also supported by numerical simulations [*Ben-Zion and Lyakhovsky*, 2006] that showed the p exponent to increase with viscosity and the thermal gradient of the crust. We thus believe that estimates of high p values for southern Iceland are not artifacts but are linked to the high geothermal gradients characteristics of these areas.

3.1. Short-Term Triggering Following the 21 June 2000 Earthquake

[34] Soon after the 21 June earthquake, seismicity rates were significantly increased. We observe short-term triggering in each of the three areas, during the first days after the 21 June earthquake. By "short-term," we mean a significant increase of seismicity rate lasting no more than a few days. All zones present a probability greater than 97% ($\gamma > 1.5$) that this short-term triggering after 21 June could not occur by pure chance (see Table 2).

[35] Note that at Árnes we cannot document any modification of the seismicity rate on 21 June. Indeed, the proximity of this area to the 21 June fault plane induced an artificial seismic gap in the database up to 22 June, most probably because of strong aftershocks occurring this day on the 21 June fault plane, and which waveforms could mask smaller events at Árnes. As a consequence, too few events were detected at Árnes on 21 June, making the estimate of $M_c(t)$ unreliable for that day. This estimate then improves on 22 June. We therefore do not estimate neither M_c nor the rate change on 21 June for the Árnes fault (see Figure 5). However, the significance of the triggering between 22 and 23 June ($\gamma = 2.5$) is a good indication that earlier triggering might have occurred there since 21 June.

[36] At Hengill, the initial triggering is significant for 1 d (see Figure 6). At Reykjanes the triggering is weaker, as suggested by smaller γ, and lasts at most 1 d (see Figure 7). This argues in favor of a correlation between distance from the main shock and duration of an initial triggering phase.

[37] The computation of static stress transfers for this sequence was performed by *Árnadóttir et al.* [2003]. According to these results, we question the ability of static stress transfers to explain these triggering episodes. First, the Hengill area is located in a stress shadow of both June

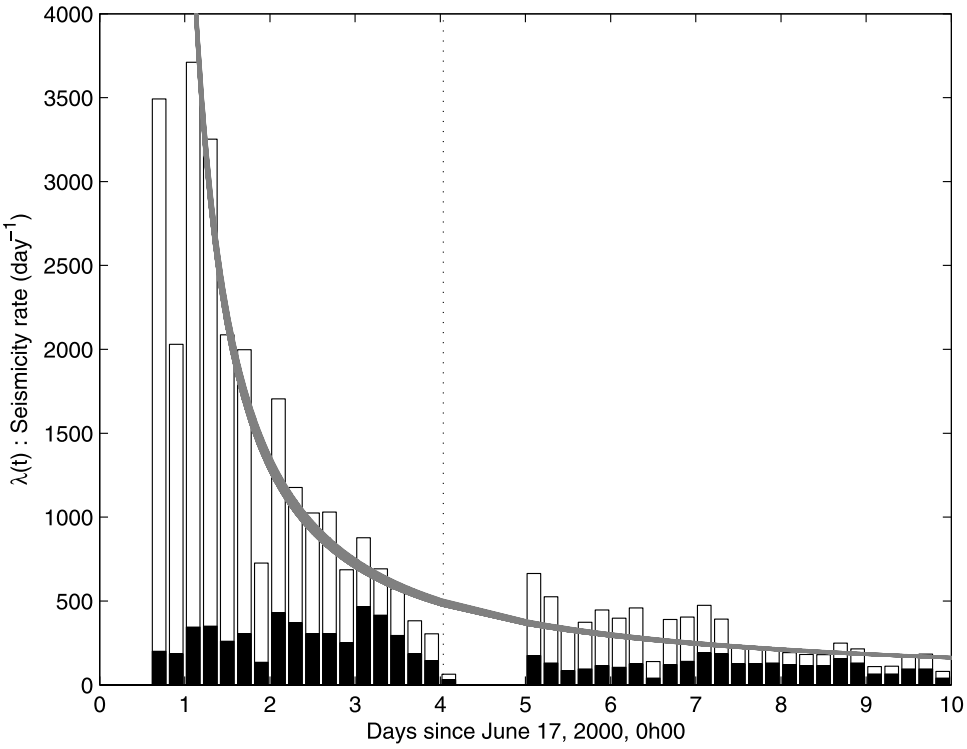

Figure 5. Seismicity rate for the Árnes fault area. Black bars indicate earthquakes detected down to $M_{\min} = 0$. White bars indicate estimation of the rate of $M \geq M_{\min}$ earthquakes, including both detected and undetected earthquakes. Grey line indicates best fit of the modified Omori formula to the data with error envelope (line thickness). An artificial gap occurs in the data between 21 and 22 June, most probably due to the high activity on the adjacent 21 June fault.

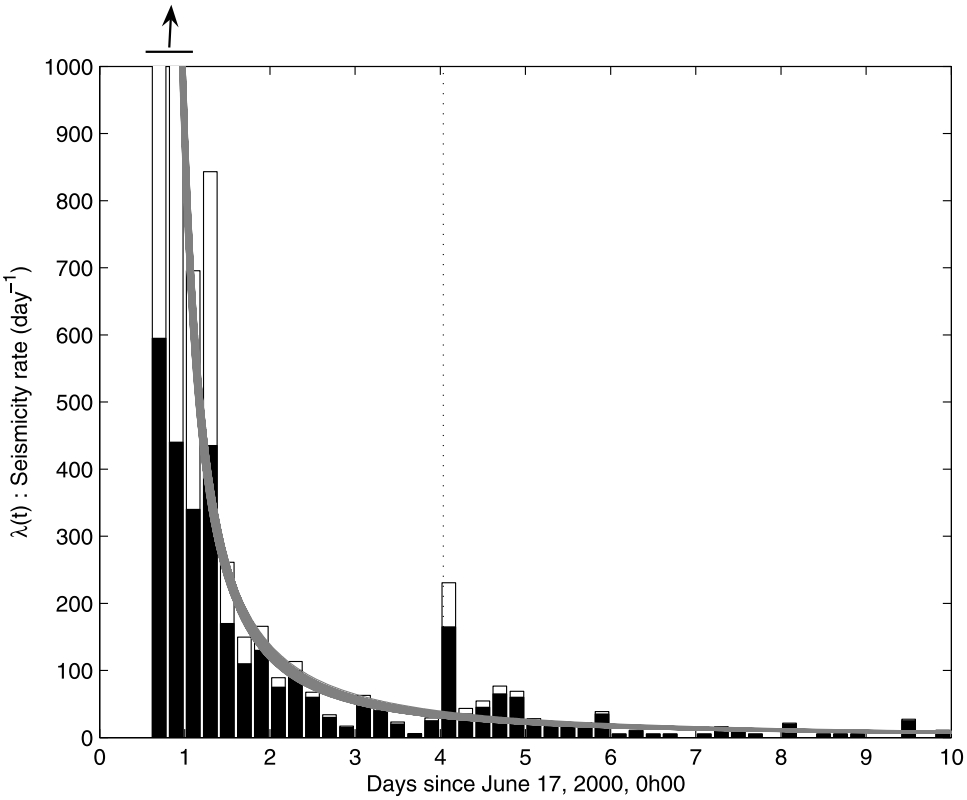

Figure 6. Same as Figure 5 for the Hengill Triple Junction area.

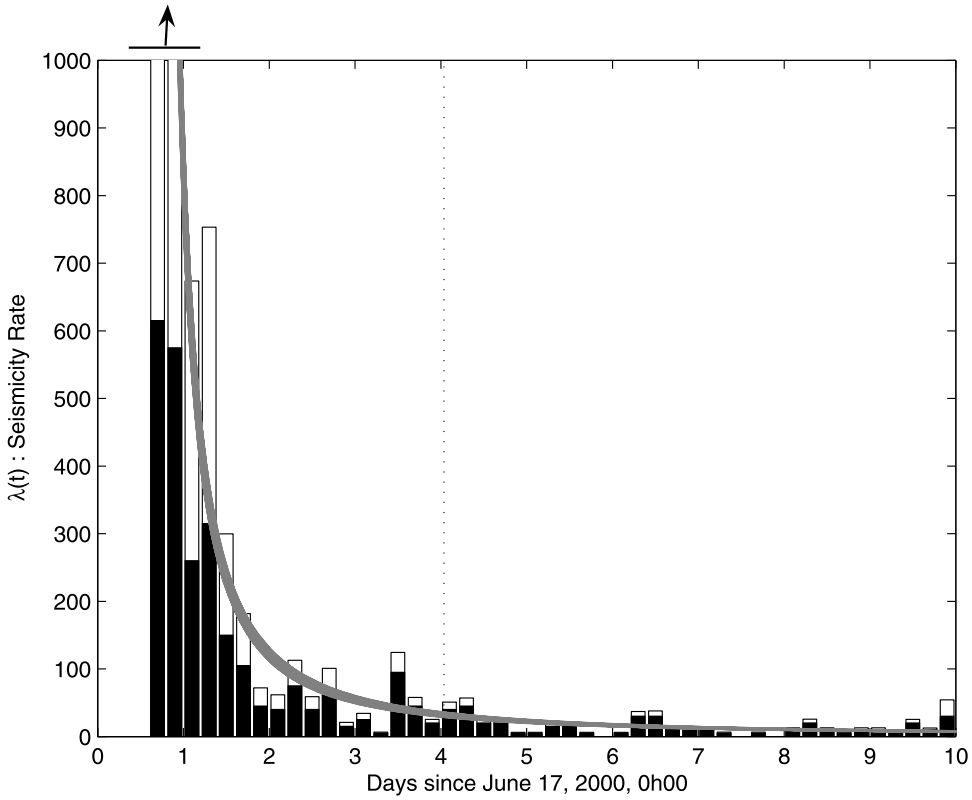

Figure 7. Same as Figure 5 for the Reykjanes Peninsula.

earthquakes (ΔCFS ~ -1 bar). Second, the Reykjanes Peninsula underwent only slight stress changes, not exceeding 0.5 bar. And third, the northern half of the Árnes fault plane was loaded whereas its southern half was unloaded by the 21 June earthquake. As seismicity rates are larger in the south than in the north, we would expect a decrease of the rates after 21 June in the Árnes area, which is not observed at the timescale of a few days. Consequently, we propose that these increases of seismicity rates at short timescale could have been triggered by ground shaking accompanying the propagation of seismic waves from the M_s6.6 21 June epicenter.

[38] Similar wave-induced perturbations have already been proposed to explain sudden episodes of triggering in southern Iceland on 17 June [*Antonioli et al.*, 2006], as well as in numerous other places after large earthquakes (see *Gomberg et al.* [2001] and *Gomberg and Johnson* [2005] for examples in the western United States). In particular, fluid-saturated (i.e., geothermal and volcanic) areas appear to react very sensitively to transient stress perturbations. The Long Valley caldera in California [*Hill et al.*, 1993; *Gomberg and Johnson*, 2005], the Yellowstone National Park in Wyoming [*Husen et al.*, 2004], or the Yalova area in Turkey [*Daniel et al.*, 2006] have all been shown, for example, to undergo significant triggering in the seconds to hours after the occurrence of a distant earthquake. The mechanical model proposed by *Silver and Valette-Silver* [1992] for geysers areas could be a valuable candidate for explaining the particular behavior of fluid-invaded regions subject to transient strains. Strain-induced microfracturing can modify the volumetric flow velocity or the reservoir permeability, and push the system out of equilibrium, thus affecting time intervals between geyser eruptions, and by extension, seismic interevent times. Nevertheless, it is still unclear how transient perturbations can affect the system for several days.

3.2. Delayed Quiescences

[39] We now investigate changes in the seismicity rates on a longer timescale, i.e., for months, up the end of year 2000. The γ values of Table 2 indicate an anomalously quiet period between 1 July and 1 October at Hengill and at Árnes. These estimates reflect the more seldom occurrence of events with $M \geq M_{\min}$ at these timescales, as compared to the predicted rate $\lambda_1^\star(t)$.

[40] At Árnes, Figures 8a and 8b show a net shutdown of activity starting about 20 d after 17 June, and lasting for about 2 months (at $\sim$80 d after 17 June, the slopes of both curves match again, indicating the end of this rate decrease). At Hengill, quiescence starts 10–15 d after 17 June, after vigorous triggering. It remains visible up to the end year 2000 (see Figure 8b).

[41] Extrapolation of $\lambda_1^\star$ to several months after the main shock predicts very low seismicity rates, possibly lower than the background rate preexisting before 17 June 2000. The method we used in this study for computing rate changes does not allow to compare these with the background rate at a longer timescale after the main shock. A complementary measure of the strength of a quiescence is provided by the comparison of mean interevent times before the seismic crisis with those during this episode, as shown on Figure 8c. Interevent times are calculated using a moving average of 20 successive of earthquakes, and values are plotted at the mean time of each window. We calculate delays between successive $M > 1$ earthquakes in order to avoid bias linked with completeness fluctuations in the catalog (such a bias remains important during the first days after 21 June, but we here focus on a later period of time). Both areas exhibit quiescences with different characteristics. After June 2000, interevent times at Hengill increase above the pre-June 2000 mean interevent time, pointing out to a clear shutdown of activity taking place after the doublet. For Árnes, the situation differs, because interevent times after June 2000 do not exceed the mean times before June 2000. In this case, the quiescence is thus only relative to the modified Omori formula prediction, and does consists in a slowdown, rather than a shutdown of activity.

[42] These observations of quiescences remind us of previous studies of earthquake sequences which showed the existence of delayed quiescence after major earthquakes. For example, *Daniel et al.* [2006] detected relative quiescence at the Yalova geothermal area, Turkey, starting 30 d after the 1999 Duzce earthquake and lasting for about 80 d. *Marsan and Daniel* [2007] also reported a significant decrease in seismicity rate in the Nansan region, that started 14 months after the 1999 Chi-Chi, Taiwan, earthquake. After the second event of the Kagoshima, Japan, doublet, *Toda and Stein* [2003] also mention a strong and long-lasting episode of quiescence. After the 1983 Coalinga earthquake, *Toda and Stein* [2002] found that the Parkfield segment of the San Andreas fault, California, experienced a quiescence that started about 6 months after this event, and lasted up to 3 years.

[43] The correlation between these quiescences in southern Iceland and static stress changes is noteworthy. As mentioned in section 3.1, both areas are expected to show a decrease in seismicity rates according to Coulomb stress calculations [*Árnadóttir et al.*, 2003]. In this context, dynamic triggering (and its respective secondary aftershocks) could be responsible for the delayed appearance of these quiescences. We can also invoke heterogeneous stress drop on fault planes obeying rate-and-state friction in order to account for such delays [*Marsan*, 2006; *Helmstetter and Shaw*, 2006].

3.3. Comparing Dynamic Triggering of Both June 2000 Main Shocks

[44] This seismic sequence was composed of two similar main shocks, of equal magnitude, nearly identical focal mechanisms, and very close location. It thus provides a unique opportunity to compare the individual effects of successive, nearly identical main shocks. It is clear that although each main shock triggered activity in southern Iceland, the second one was far less efficient in doing so. A remarkable feature of this sequence is the importance of triggering at remote locations from the two ruptures. Following 17 June, seismic activity was promoted up to 80 km away from the Árnes fault plane. Some of the events triggered had relatively high magnitude [*Pagli et al.*, 2003; *Antonioli et al.*, 2006], and themselves generated many aftershocks.

[45] After the 21 June main shock, seismicity increased at the Hengill Triple Junction and on the Reykjanes Peninsula, which are both outside the main rupture zone, and are therefore likely to be related to dynamic triggering. The

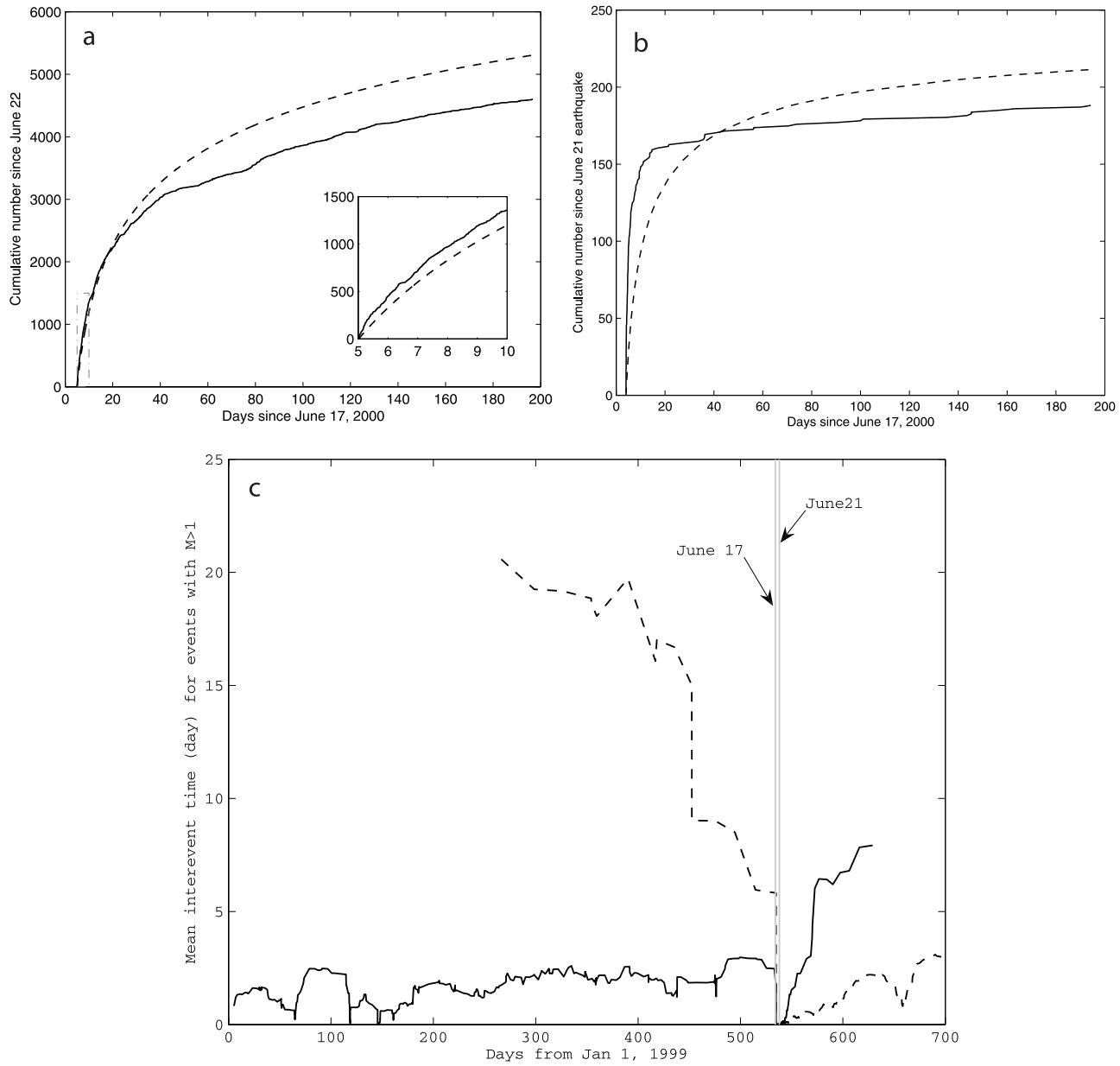

Figure 8. Long-term quiescences. (top) Comparison between the extrapolated rate of earthquakes $\lambda_0(t)$ up to the end of year 2000 and the rate $\lambda_1^\star$ of earthquakes for magnitudes $M \geq M_{\min}$, for (a) the Árnes fault area and (b) the Hengill Triple Junction. (c) Mean interevent times between successive $M > 1$ earthquakes. The interevent times are averaged over 20 successive couples of earthquakes, for the Hengill area (black line) and for the Árnes area (dashed line). The double vertical bars correspond to the occurrence of both June 2000 main shocks.

effect of this transient perturbation vanishes quickly (after 1 or 2 d) (see Table 2).

[46] We now examine the relationship between the number of events triggered by each main shock over 3 d and the dynamic stress perturbation for these two zones. In order to separate each main shock contribution to the aftershock sequence, we adjust the seismicity rates to a double Omori-Utsu law, with a first trigger occurring at $t = 0$ (on 17 June), and a second one at t_2,

$$\lambda(t) = \frac{K}{(t-c)^p} + \frac{K_2}{(t-t_2+c)^{p_2}} \tag{13}$$

where all 2-subscripted parameters are related to the second trigger. Values obtained for these parameters are listed in Table 1. Individual main shock productivity Q_i (in number of triggered events in the first 3 d) is calculated according to the following equations:

$$Q_1 = \int_0^{3d} \frac{K}{(t+c)^p}\,dt \tag{14}$$

$$Q_2 = \int_{t_2}^{t_2+3d} \frac{K_2}{(t-t_2+c)^{p_2}}\,dt \tag{15}$$

Table 3. Estimation of the Main Shock Respective Productivities and the Corresponding Productivity Over Peak Shear Dynamic Stress Ratios[a]

	Hengill	Reykjanes
Q_1	5653	5450
Q_2	49	12
σ_1^d	1.52	0.74
$\sigma_2^d - \sigma_1^d$	0.62	0.61
Q_1/σ_1^d	3719	7365
$Q_2^{ex} = (Q_1/\sigma_1^d)(\sigma_2^d - \sigma_1^d)$	2306	4493
Q_2/Q_2^{ex}	2.1%	0.3%

[a]Productivities Q_i are expressed in number of events triggered in the first 3 d following the main shock and peak shear stresses in bars. The quantity Q_2^{ex} corresponds to the expected productivity of triggered events with a simple stress-threshold model of dynamic triggering.

We then compare these values with the peak shear dynamic stress for each area. Modeling of dynamic stress transfers is performed using the discrete wave number method [*Bouchon*, 1981; *Cotton and Coutant*, 1997]. The kinematic fault slip model obtained by *Pedersen et al.* [2003] from joint inversion of InSAR and GPS data is used as input for the modeling. We use the four-layer velocity model of *Antonioli et al.* [2006] and *Vogfjord et al.* [2002], and we adopt a risetime of 1 s. The dynamic stresses are evaluated at the central point of each area (see Figure 1). From these, two values are estimated: σ_1^d, which corresponds to the peak shear dynamic stress amplitude produced by the first main shock, and $\sigma_2^d - \sigma_1^d$, which corresponds to the excess of peak shear dynamic stress of the second event relatively to the first one. Our simulations lead to σ_1^d and σ_2^d values of the same order (few bars), as expected from the similarity of both main shocks. Peak dynamic stresses of the 17 June earthquake, as presented in Table 3, are in good agreement with estimates of *Antonioli et al.* [2006]. Moreover, values for σ_2^d are greater than σ_1^d because the second main shock was closer to the target areas.

[47] We then compare this last value with the productivity Q_2^{ex} that would be expected from a simple stress threshold rupture model, as sketched in Figure 9:

$$Q_2^{ex} = \frac{Q_1}{\sigma_1^d}\left(\sigma_2^d - \sigma_1^d\right) \tag{16}$$

Such a basic model predicts that for instance, under a 1 bar stress perturbation, all faults that are within 1 bar from their failure threshold will fail. Note that we could not assess an approximative peak dynamic stress value for the Árnes area, as this area is located in the near field of the 17 June earthquake.

[48] Values of Table 3 clearly indicate that this simple model does not hold, as productivities Q_2 for Hengill and Reykjanes after the 21 June main shock are 2.1% and 0.3%, respectively, of what could be expected from the first main shock of the sequence. This result is in agreement with *Árnadóttir et al.* [2003], who pointed out this low productivity after the 21 June event, although it occurred closer to these areas.

[49] This discrepancy in productivity is also reflected in seismic moment releases associated with each main shock. We estimate seismic moment release from magnitude (M_L) of events of the catalog using the relation of *Hanks and Kanamori* [1979] for moment magnitudes

$$M_o = 10^{1.5(M_L+10.7)} \tag{17}$$

This measure is dominated by aftershocks with large magnitudes, and thus is not sensitive to fluctuations of the detection threshold. At Reykjanes, only 0.1% of the post-17 June moment release is observed after the second earthquake, and this value slightly increases to 3.6% at Hengill. Two reasons can explain this low productivity Q_2: (1) the distribution of stress $f(\sigma)$ is not uniform, but "bell-shaped" close to σ_c so that there is an anomalously large number of faults sufficiently close to failure prior to the June 2000 crisis. This would imply that the whole of the SISZ was actually close to failure at the same time. The capacity of this region to produce earthquake sequences [*Einarsson and Eiríksson*, 1982; *Árnadóttir et al.*, 2001; *Bergerat*, 2001] is perhaps a signature of such a regionally wide loading process. (2) The supposed proportionality (linearity) between σ^d and Q is not valid. An alternative could be that the first main shock depleted the population of faults available for rupture, so that a quiescence eventually emerge by lack of usable faults. However, we have no idea how to test this model, i.e., how to estimate in an independent way the number of usable faults prior to the occurrence of the first main shock. *Johnson and Jia* [2005] and *Gomberg and Johnson* [2005] proposed a model for dynamic triggering based on laboratory experiments, which predicts that propagation of seismic waves modifies the physical state of faults with gouge, according to dynamic nonlinear elasticity. After the passing of waves, the system recovers slowly, implying that strength of the next triggering episode will depend on the degree of recovery, i.e., on time elapsed since the preceding episode.

4. Conclusion

[50] Using data recorded by the SIL seismological network from June to December 2000, we have studied

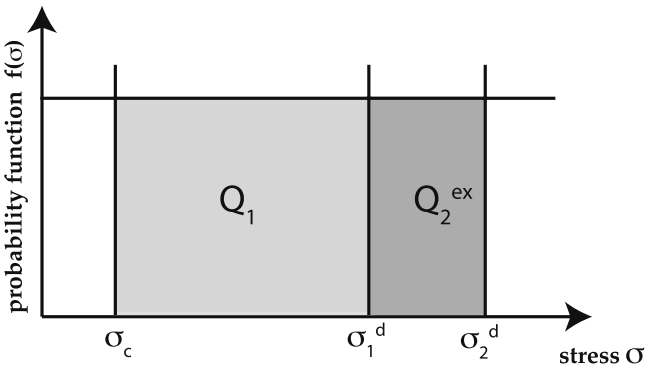

Figure 9. A simple model with stress threshold σ_c. The probability density $f(\sigma)$ of the stress σ is uniform, so that the seismicity rate due to a constant tectonic loading stress rate is also constant. At the time of the first main shock, a proportion Q_1 of events are triggered by the dynamic stress σ_1^d. Neglecting the tectonic loading between the times of the two main shocks, this model predicts a proportion $Q_2^{ex} = (Q_1/\sigma_1^d)(\sigma_2^d - \sigma_1^d)$ of earthquakes dynamically triggered by the second main shock.

earthquake interactions during the June 2000 seismic crisis in Iceland. We focused on the impact of the second, M_s 6.6, 21 June main shock on the preexisting seismicity. For this purpose, we developed a method that accounts for the rapid fluctuations of the network detection threshold. Compared to an analysis with constant M_c, this approach optimizes available information, using all events of a catalog down to a given magnitude $M_{\min}$, lower than the smallest cutoff magnitude. For three areas, we considered the Omori-Utsu decay of aftershocks after 17 June as a nonstationary reference seismicity rate, and we investigated departures from this general trend after the second main shock.

[51] Vigorous instantaneous triggering of seismicity is observed on the Reykjanes Peninsula, at Hengill, and on the Árnes fault plane after the 21 June earthquake. We associate these perturbations with dynamic propagation of stresses in the crust, especially for the former two regions which are clearly off the main rupture zone. Quiescences delayed for 10 to 20 d after the second main shock were also detected at Hengill and on the Árnes fault plane. At Hengill, this quiescence remains significant at least up to the end of year 2000. We mentioned that long-term quiescences for these two areas are more consistent with Coulomb stress calculations than the preceding short-term triggering. This pattern of initial triggering followed by quiescence can be explained in static stress shadows by either dynamic triggering, or static stress spatial heterogeneity, dominating the seismicity dynamics at early times (as observed for the 1999 Chi-Chi earthquake [see *Marsan and Daniel*, 2007]).

[52] We also compared the individual effects of each main shock on the regional seismicity over a timescale of 3 d, for which the initial triggering, likely to be dynamic, dominates. Surprisingly, despite similar magnitude and focal mechanism, the second main shock triggered far less events than the first one. Only few percent of the number of aftershocks expected from a simple stress threshold model of dynamic triggering occurred. This observation is consistent with estimates of seismic moment release after each main shock.

[53] This result implies that either (1) stress distribution is not uniform in the SISZ or (2) the scaling of aftershock productivities with peak dynamic stress amplitudes is not valid.

[54] In the current context of early warning for main shocks/aftershocks, it is of first importance to understand the physical phenomenon driving the production of triggered events after a main shock. In this respect, this analysis reveals the nonlinear character of aftershock production induced by dynamic triggering. For at least some days, this nucleation process could thus ''keep in memory'' the occurrence of a previous short-lived perturbation (few seconds).

[55] **Acknowledgments.** We thank Kristin Vodfjord, Rikke Pedersen, and the staff of the Icelandic Meteorological Office for providing seismic data and information about catalogues. We also thank the Associate Editor and the two referees for their critical reviews, which helped to improve the manuscript.

References

Antonioli, A., M. E. Belardinelli, A. Bizzarri, and K. S. Vogfjord (2006), Evidence of instantaneous dynamic triggering during the seismic sequence of year 2000 in south Iceland, *J. Geophys. Res.*, *111*, B03302, doi:10.1029/2005JB003935.

Árnadóttir, T., S. Hreinsdóttir, G. Gudmundsson, P. Einarsson, M. Heinert, and C. Völksen (2001), Crustal deformation measured by GPS in the South Iceland Seismic Zone due to two large earthquakes in June 2000, *Geophys. Res. Lett.*, *28*(21), 4031–4033.

Árnadóttir, T., S. Jónsson, R. Pedersen, and G. Gudmundsson (2003), Coulomb stress changes in the South Iceland Seismic Zone due to two large earthquakes in June 2000, *Geophys. Res. Lett.*, *30*(5), 1205, doi:10.1029/2002GL016495.

Árnadóttir, T., H. Geirsson, and P. Einarsson (2004), Coseismic stress changes and crustal deformation on the Reykjanes Peninsula due to triggered earthquakes on 17 June 2000, *J. Geophys. Res.*, *109*, B09307, doi:10.1029/2004JB003130.

Ben-Zion, Y., and V. Lyakhovsky (2006), Analysis of aftershocks in a lithospheric model with seismogenic zone governed by damage rheology, *Geophys. J. Int.*, *165*, 197–210, doi:10.1111/j.1365-246X.2006.02878.x.

Bergerat, F. (2001), La sismicité historique en Islande: Aspects géologiques et impacts environnementaux et sociaux. Exemples dans la Zone sismique sud-islandaise, *C.R. Acad. Sci., Ser. 2*, *333*, 81–92.

Bohnenstiehl, D., M. Tolstoy, R. Dziak, C. Fox, and D. Smith (2002), Aftershock sequences in the mid-ocean ridge environment: An analysis using hydroacoustic data, *Tectonophysics*, *354*(1), 49–70.

Bouchon, M. (1981), A simple method to calculate Green's functions in elastic layered media, *Bull. Seismol. Soc. Am.*, *71*, 959–971.

Clifton, A., C. Pagli, J. Jónsdóttir, K. Eythorsdóttir, and K. Vogfjör (2003), Surface effects of triggered fault slip on Reykjanes Peninsula, SW Iceland, *Tectonophysics*, *369*, 145–154.

Cotton, F., and O. Coutant (1997), Dynamic stress variations due to shear faults in a plane-layered medium, *Geophys. J. Int.*, *128*, 676–688.

Daniel, G., D. Marsan, and M. Bouchon (2006), Perturbation of the Izmit earthquake aftershock decaying activity following the 1999 M_w 7.2 Düzce, Turkey, earthquake, *J. Geophys. Res.*, *111*, B05310, doi:10.1029/2005JB003978.

Das, S., and C. Scholz (1981), Off-fault aftershock clusters caused by shear stress increase?, *Bull. Seismol. Soc. Am.*, *71*(5), 1669–1675.

Einarsson, P. (1991), Earthquakes and present-day tectonism in Iceland, *Tectonophysics*, *189*, 261–279.

Einarsson, P., and J. Eiríksson (1982), Earthquake fractures in the districts Land and Rangárvellir in the South Iceland Seismic Zone, *Joekull*, *32*, 113–120.

Felzer, K. R., and E. E. Brodsky (2005), Testing the stress shadow hypothesis, *J. Geophys. Res.*, *110*, B05S09, doi:10.1029/2004JB003277.

Gomberg, J., and P. Johnson (2005), Dynamic triggering of earthquakes, *Nature*, *437*, 830.

Gomberg, J., P. Reasenberg, P. Bodin, and R. Harris (2001), Earthquake triggering by seismic waves following the Landers and Hector Mine earthquakes, *Nature*, *411*, 462–466.

Gutenberg, B., and C. Richter (1954), *Seismicity of the Earth and Associated Phenomena*, Princeton Univ. Press, Princeton, N.J.

Hanks, T., and H. Kanamori (1979), A moment magnitude scale, *J. Geophys. Res.*, *84*(B5), 2348–2350.

Helmstetter, A., and B. E. Shaw (2006), Relation between stress heterogeneity and aftershock rate in the rate-and-state model, *J. Geophys. Res.*, *111*, B07304, doi:10.1029/2005JB004077.

Helmstetter, A., Y. Kagan, and D. Jackson (2006), Comparison of short-term and time-independent earthquake forecast models for southern California, *Bull. Seismol. Soc. Am.*, *96*(1), 90–106, doi:10.1785/0120050067.

Hill, D., P. Reasenberg, A. Michael, and W. Arabaz (1993), Seismicity remotely triggered by the Mw7.3 Landers, California, earthquake, *Science*, *260*, 1617–1623.

Husen, S., S. Wiemer, and R. Smith (2004), Remotely triggered seismicity in the Yellowstone National Park region by the 2002 M_w = 7.9 Denali fault earthquake, Alaska, *Bull. Seismol. Soc. Am.*, *94*(6B), S317–S331, doi:10.1785/0120040617.

Jakobsdóttir, S. (2006), The SIL system—15 years of near-real time monitoring, paper presented at First European Conference on Earthquake Engineering and Seismology, Eur. Assoc. of Earthquake Eng., Geneva, Switzerland.

Johnson, P., and X. Jia (2005), Nonlinear dynamics, granular media and dynamic earthquake triggering, *Nature*, *437*, 871–874.

Kagan, Y., and L. Knopoff (1981), Stochastic synthesis of earthquake catalogs, *J. Geophys. Res.*, *86*, 2856–2862.

King, G., and M. Cocco (2000), Fault interactions by elastic stress changes: New clues from earthquakes sequences, *Adv. Geophys.*, *44*, 1–38.

Klein, F. W., T. Wright, and J. Nakata (2006), Aftershock decay, productivity, and stress rates in Hawaii: Indicators of temperature and stress from magma sources, *J. Geophys. Res.*, *111*, B07307, doi:10.1029/2005JB003949.

Mallman, E. P., and M. D. Zoback (2007), Assessing elastic Coulomb stress transfer models using seismicity rates in southern California and south-

western Japan, *J. Geophys. Res.*, *112*, B03304, doi:10.1029/2005JB004076.
Marsan, D. (2003), Triggering of seismicity at short timescales following Californian earthquakes, *J. Geophys. Res.*, *108*(B5), 2266, doi:10.1029/2002JB001946.
Marsan, D. (2006), Can coseismic stress variability suppress seismicity shadows? Insights from a rate-and-state friction model, *J. Geophys. Res.*, *111*, B06305, doi:10.1029/2005JB004060.
Marsan, D., and G. Daniel (2007), Measuring the heterogeneity of the coseismic stress change following the 1999 M_w7.6 Chi-Chi earthquake, *J. Geophys. Res.*, *112*, B07305, doi:10.1029/2006JB004651.
Marsan, D., and O. Lengliné (2008), Extending earthquakes' reach through cascading, *Science*, *319*, 1076–1079, doi:10.1126/science.1148783.
Marsan, D., and S. Nalbant (2005), Methods for measuring rate changes: A review and a study of how the M_w7.3 Landers earthquake affected the aftershock sequence of the M_w6.1 Joshua Tree earthquake, *Pure Appl. Geophys.*, *162*, 1151–1185.
Ogata, Y., and K. Katsura (1993), Analysis of temporal and spatial heterogeneity of magnitude frequency distribution inferred from earthquake catalogues, *Geophys. J. Int.*, *113*, 727–738.
Ogata, Y., and K. Katsura (2006), Immediate and updated forecasting of aftershock hazard, *Geophys. Res. Lett.*, *33*, L10305, doi:10.1029/2006GL025888.
Omori, F. (1894), On the aftershocks of earthquakes, *J. Coll. Sci. Imp. Univ. Tokyo*, *7*, 111–200.
Pagli, C., R. Pedersen, F. Sigmundsson, and K. L. Feigl (2003), Triggered fault slip on June 17, 2000 on the Reykjanes Peninsula, SW-Iceland captured by radar interferometry, *Geophys. Res. Lett.*, *30*(6), 1273, doi:10.1029/2002GL015310.
Parsons, T. (2002), Global Omori law decay of triggered earthquakes: Large aftershocks outside the classical aftershock zone, *J. Geophys. Res.*, *107*(B9), 2199, doi:10.1029/2001JB000646.
Pedersen, R., S. Jónsson, T. Árnadóttir, F. Sigmundsson, and K. Feigl (2003), Fault slip distribution of two June 2000 M_w6.5 earthquakes in south Iceland estimated from joint inversion of InSAR and GPS measurements, *Earth Planet. Sci. Lett.*, *213*, 487–502.
Ringdal, F. (1975), On the estimation of seismic detection thresholds, *Bull. Seismol. Soc. Am.*, *65*(6), 1631–1642.
Silver, P., and N. Valette-Silver (1992), Detection of hydrothermal precursors to large northern California earthquakes, *Science*, *257*, 1363–1367.
Stefánsson, R., G. G. Munsson, and P. Halldórsson (2003), The south Iceland earthquakes 2000: A challenge for earthquake prediction research.
Toda, S., and R. S. Stein (2002), Response of the San Andreas fault to the 1983 Coalinga-Nuñez earthquakes: An application of interaction-based probabilities for Parkfield, *J. Geophys. Res.*, *107*(B6), 2126, doi:10.1029/2001JB000172.
Toda, S., and R. Stein (2003), Toggling of seismicity by the 1997 Kagoshima earthquake couplet: A demonstration of time-dependent stress transfer, *J. Geophys. Res.*, *108*(B12), 2567, doi:10.1029/2003JB002527.
Utsu, T. (1961), A statistical study on the occurrence of aftershocks, *Geophys. Mag.*, *30*(4), 521–605.
Vogfjord, K., et al. (2002), Crustal profiling in Iceland using earthquake source-arrays, *Eos Trans. AGU*, *83*(47), Fall Meet. Suppl., Abstract S61C-1161.
Wiemer, S., and K. Katsumata (1999), Spatial variability of seismicity parameters in aftershock zones, *J. Geophys. Res.*, *104*(B6), 13,135–13,151, doi:10.1029/1999JB900032.
Wiemer, S., S. McNutt, and M. Wyss (1998), Temporal and three dimensional spatial analyses of the frequency-magnitude distribution near Long Valley Caldera, California, *Geophys. J. Int.*, *134*(2), 409–421, doi:10.1046/j.1365-246x.1998.00561.x.
Wyss, M., and R. Stefánsson (2006), Nucleation points of recent mainshocks in southern Iceland, mapped *b*-values, *Bull. Seismol. Soc. Am.*, *96*(2), 599–608, doi:10.1785/0120040056.

M. Bouchon and G. Daniel, Laboratoire de Geophysique Interne et Tectonophysique, CNRS - Université Joseph Fourier, BP 53, F-38041 Grenoble Cedex 9, France. (guillaume.daniel@obs.ujf-grenoble.fr)

D. Marsan, Laboratoire de Geophysique Interne et Tectonophysique, CNRS - Université de Savoie, Campus scientifique, F-73376 Le Bourget du Lac Cedex, France.